# Synthesis and Characterization of Novel Diethylenetriamine Based Sulfonamide Ligands and Their Bidentate Platinum(II) Complexes Toward Anticancer Drug Leads

Dinithi Kaluthanthiri,[1,2] Umapriyatharshini Rajagopalan,[3] Sameera Samarakoon,[3] Laksiri Weerasinghe,[1] Inoka C. Perera[4] and Theshini Perera*[1]

[1] *Department of Chemistry, Faculty of Applied Sciences, University of Sri Jayewardenepura, Sri Lanka,* [2] *Department of Pharmacy and Pharmaceutical Sciences, Faculty of Allied Health Sciences, University of Sri Jayewardenepura, Sri Lanka*[3]*, Institute of Biochemistry, Molecular Biology and Biotechnology, University of Colombo, Sri Lanka.* [4] *Department of Zoology and Environment Sciences, Faculty of Science, University of Colombo, Sri Lanka*
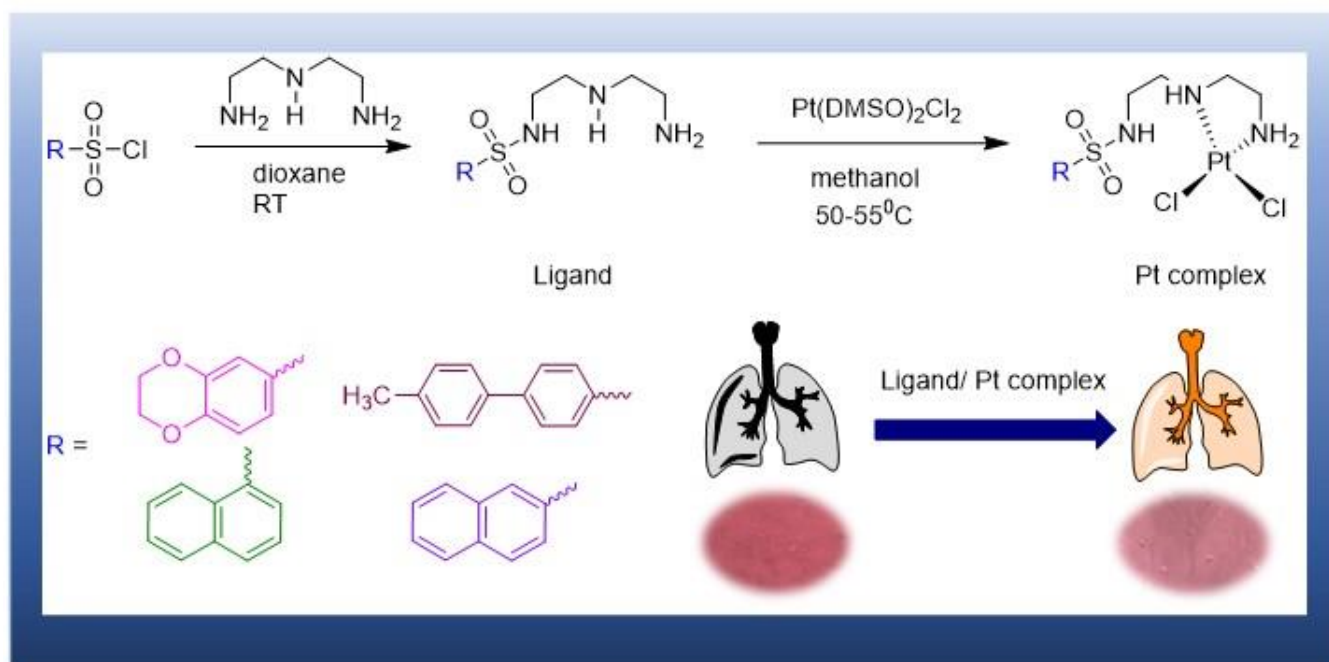
Abstract

Diethylenetriamine (dienH) is one of the most biologically compatible chelate frameworks. Its hydrophilic amine moiety was functionalized via *N*-sulfonylation with sulfonyl chloride to produce two novel ligands; $N(SO_2)$(bzd)dienH (L1) and $N(SO_2)$(4-Mebip)dienH (L2) and two reported ligands; $N(SO_2)$(1-nap)dienH (L3) and $N(SO_2)$(2-nap)dienH (L4). Treatment of *cis*-Pt(DMSO)$_2$Cl$_2$ with L1, L2, L3 and L4 afforded four novel neutral complexes [Pt($N(SO_2)$(bzd)dienH)Cl$_2$] (C1), [Pt($N(SO_2)$(4-Mebip)dienH)Cl$_2$] (C2), [Pt($N(SO_2)$(1-nap)dienH)Cl$_2$] (C3) and [Pt($N(SO_2)$(2-nap)dienH)Cl$_2$] (C4) respectively. All synthesized compounds were characterized by ^{1}H NMR, UV-Vis, FTIR and fluorescence spectroscopy. Aliphatic diethylenetriamine protons of the ligands appeared in the 3.00 -2.30 ppm region in ^{1}H NMR spectra recorded in DMSO-d_6. Upon complexation, the appearance of two broad NH peaks between 5.00 -7.00 ppm region and another broad peak between 7.00-8.00 ppm confirmed the bidentate denticity of the ligands vs tridentate. The formation of metal complexes was further supported by FTIR spectra in which the S-N stretching band for the metal complexes appears at lower wavenumbers compared to that of the corresponding free ligands. Emission spectra were recorded in methanol and intense fluorescence properties were observed in the 331-364 nm range for the ligands, whereas the corresponding Pt complexes showed quenched fluorescence. *In vitro* cytotoxic effects were investigated using sulforhodamine B assay, where L2 (< 10 µg/mL) demonstrated increased levels of cytotoxicity followed by C2 (< 25 µg/mL) and C4 (< 50 µg/mL) to non-small cell lung cancer cells in dose and time-dependent manner, with less or no cytotoxic effects to normal lung cells tested. Among the compounds tested, C1 and C3 displayed comparatively lower but more potent cytotoxic effects on lung cancer cells. Notably, these compounds did not exhibit any toxicity towards normal cells. Thus, they hold promise as lead compounds for the development of chemotherapeutic agents targeting lung cancer.

Keywords: Platinum, Sulfonamide, Biphenyl, Benzodioxan, aphthalene

1.   Introduction

Although many medications are currently available for various human diseases, the search for novel efficacious and safe therapeutic agents is a continuous and never-ending process. Various metal ions play a dynamic role in biological systems, and currently, many metal-based compounds are used as therapeutics and diagnostic tools. The therapeutic approach of metallo compounds is identified as bearing two main arms; ligands as drugs that target metal ions in some form, and metal-based drugs and imaging agents where the central metal ion is usually the key feature of the mechanism of action (Farrell, 2003).

The discovery of *cis*-diamminedichloroplatinum(II), cisplatin was a remarkable achievement in medicinal chemistry and a heavenly answer for cancer patients (Wang and Lippard, 2005a). Cisplatin has established itself as a chemotherapeutic agent for the treatment of testicular, lung, ovarian and bladder cancers (Wang and Lippard, 2005a). Pt complexes have the advantages of low oxidation number and favourable binding to selected soft centres of biomolecules (Wang and Lippard, 2005a). Particularly, Pt(II) agents target the nucleus of cancer cells, which has a high affinity towards N7 of purine bases, predominantly in guanine. Despite its high efficacy, cisplatin induces undesirable side effects such as nephrotoxicity, neurotoxicity and nausea (Wang and Lippard, 2005a). We were motivated to search for new platinum compounds which possess promising anticancer properties and while eliminating severe side effects.

N-sulfonamides have been originally identified as an antibacterial agent, and many other activities were discovered later on as anticonvulsants (Wolff, 1996), carbonic anhydrase inhibitors (Chegwidden et al., 2013), microtubule inhibitors (Mohan et al., 2006) and histone deacetylase inhibitors (Fournel et al., 2002). Therefore, incorporating *N*-sulfonamides into platinum complexes provides promising antiproliferative activity (Alemán et al., 2011). Limited literature is available on the platinum complexes of aliphatic polyamine sulfonamide ligand along with their biological assay evaluation. Jose and coworkers first reported the anticancer properties of platinum *N*-sulfonamide complexes with different aliphatic amines in *trans* geometry (Alemán et al., 2011). Christoforou et al. have shown the bidentate, tridentate and quadridentate properties of diethylenetriamine sulfonamide ligand to produce *cis*-platinum(II) complexes and reported their interactions with 5-GMP and methionine (Christoforou et al., 2006).

In this study, we report two novel diethylenetriamine-based sulfonamide ligands and four novel bidentate *cis*-platinum(II) complexes (Figure 1). The ligands were synthesized via *N*-sulfonylation of one terminal amine group of diethylenetriamine which resulted in yielding *N*(SO$_2$R)dienH type ligands (The H indicates the protons displaceable upon Pt complexation). We utilized four potent fluorophores as R groups; 1,4-benzodioxan, 4-methylbiphenyl, 1-naphthalene and 2-naphthalene to yield *N*(SO$_2$)(bzd)dienH (L1), *N*(SO$_2$)(4-Mebip)dienH (L2), *N*(SO$_2$)(1-nap)dienH (L3) and *N*(SO$_2$)(2-nap)dienH (L4) respectively. The L3 and L4 ligands have been previously reported, and their Re (I) tricarbonyl complexes have shown promising cytotoxic towards lung cancer (Darshani et al., 2020a).

Unlike a more hydrophobic dipicolylamine ligand system i.e; *N*(SO$_2$R)dpa, diethylenetriamine ligand system is more hydrophilic, more flexible and ideal for bio-conjugation (Christoforou et al., 2006). This aliphatic linear triamine backbone is stable to bases and, more importantly, compatible with bioconjugation due to its small size. Literature evidence is available for the instability of the coordinated *N*(SO$_2$R)dpa ligand system due to easy access to methylene groups for the bases (Abhayawardhana et al., 2014). Our ligand system, *N*H(CH$_2$CH$_2$NH$_2$)$_2$ also possesses the CH$_2$NH$_2$ group, which has low electrophilicity and is stable for attack by bases. Moreover, its relative hydrophilicity property is more attractive for possible application in radio kit preparations. Though diethylenetriamines are examples of the NNN donor system, the synthesized *N*(SO$_2$R)dienH ligands may serve either as bidentate ligands (Central N and one terminal N) or tridentate upon Pt(II) complexation. A previous study has demonstrated the different ligand binding modes of DNSH-dienH (DNSH=5-(dimethylamino)naphthalene) to platinum as well as their interactions with biomolecules; 5'-GMP, 3'-IMP, 9-ethylguanine and sulfur of methionine (Christoforou et al., 2006). In this study our focus has been to explore the anticancer properties of charged Pt complexes having dangling sulfonamide groups.

Cancer continues to be a significant global cause of mortality, with lung cancer ranking as the second most prevalent cancer worldwide (Siegel et al., 2023).. The anticancer potential of L3,L4 and their Re(CO)$_3$ complexes against non-small lung cancer observed in the study conducted by Darshani et al (Darshani et al., 2020b). Given the crucial role of platinum-based anticancer drugs in diverse cancer treatments (Wang and Lippard, 2005b), including Non-Small Cell Lung Cancer (Zhu et al., 2019, Rossi and Di Maio, 2016), our research was formulated to investigate the antitumor potential of four novel Platinum(II) complexes and two new ligands. Furthermore, we assessed the drug-likeness of the ligands to gain insight into their therapeutic potential, which is closely linked to their cytotoxic effects.
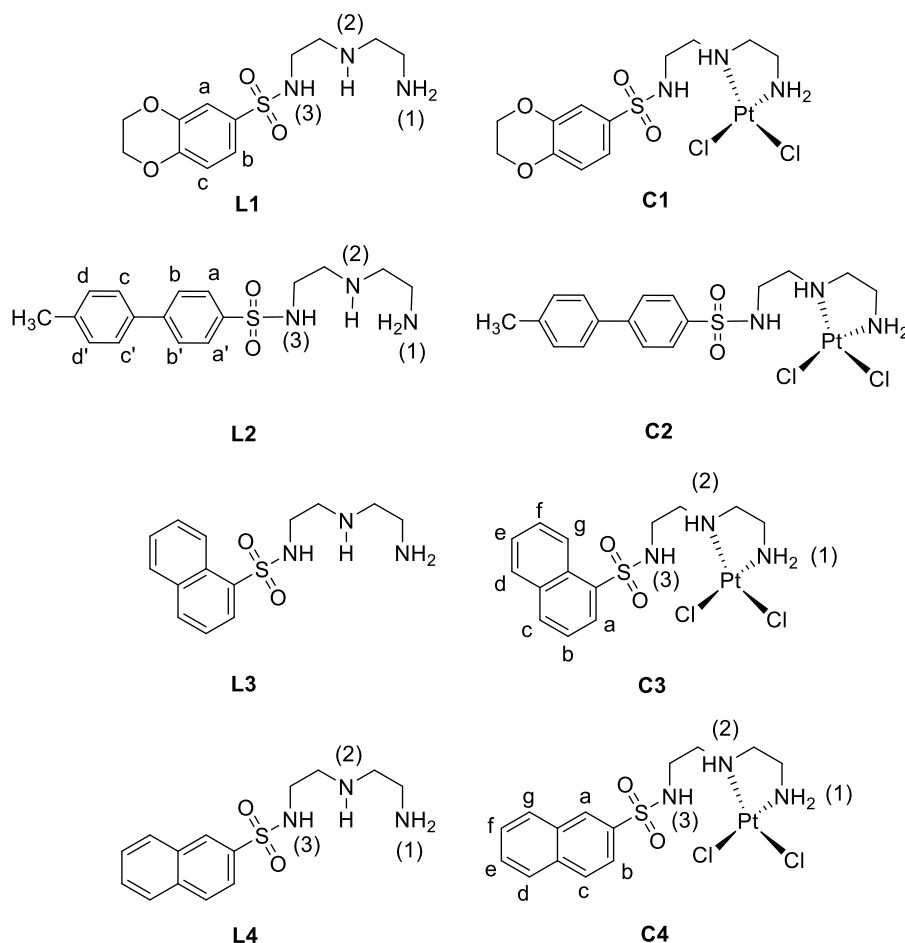
Figure 1: Proposed ligands $N(SO_2)(bzd)dienH$ (L1), $N(SO_2)(4\text{-Mebip})dienH$ (L2), $N(SO_2)(1\text{-nap})dienH$ (L3), $N(SO_2)(2\text{-nap})dienH$ (L4) and the complexes $[Pt(N(SO_2)(bzd)dienH)Cl_2]$ (C1), $[Pt(N(SO_2)(4\text{-Mebip})dienH)Cl_2]$ (C2), $[Pt(N(SO_2)(1\text{-nap})dienH)Cl_2]$ (C3) and $[Pt(N(SO_2)(2\text{-nap})dienH)Cl_2]$ (C4)

2. Experimental

2.1. Starting materials

1,4-benzodioxan-6-sulfonyl chloride ((bzd)SO$_2$Cl), 4-methylbiphenyl-4-sulfonyl chloride ((4-Mebip)SO$_2$Cl), 1-naphthalenesulfonyl chloride ((1-nap)SO$_2$Cl), 2-naphthalenesulfonyl chloride ((2-nap)SO$_2$Cl), diethylenetriamine (dienH), K$_2$PtCl$_4$, 1,4-dioxane, chromasolv water, methanol and dichloromethane were used as received from Sigma-Aldrich. *cis*-Pt(DMSO)$_2$Cl$_2$ was prepared by a known method (Price et al., 1972).

2.2. Methodology

2.2.1. Instrumentation

Ligands and metal complexes formation was assessed with TLC performances. UV-Vis absorption spectra were obtained using a GENESIS 10S UV-Vis spectrophotometer. UV-Vis absorption spectra were obtained in methanol with baseline correction. The Fourier transform infrared spectra were recorded in Thermo Scientific NICOLET iS10 spectrometer. ATR spectra were obtained in the range of 400-4000 cm^{-1}. Data were processed with UV WIN software. Spectra were obtained in methanol with baseline

correction. Fluorescence spectra were obtained in methanol on a Thermo Scientific Lumina spectrophotometer using a 150W Xenon arc lamp as the excitation source. Data were processed with Luminous software. Solutions were prepared by dissolving the analyte in methanol. ^{1}H NMR spectra were recorded on a Bruker 400 MHz spectrometer in DMSO-d_6. Peak positions are relative to residual DMSO-d_6 signal, and the data were analysed with MestReNova software.

2.2.2. General Synthesis of (N(SO₂R)dienH ligands

A solution of sulfonyl chloride (5 mmol) in 100 ml of dioxane was added dropwise over 2 h to a solution of *N*(H)diene (50 mmol) in 100 ml dioxane. The reaction mixture was stirred overnight at room temperature. After reaction completion, as evident from TLC, the product was extracted into CH_2Cl_2 (2 x 100ml) and the solvent was removed under rotary evaporation.

2.2.2.1. Synthesis of (N(SO₂)(bzd)dienH ligand (L1)

As described in the general procedure, with 1,4-benzodioxan-6-SO₂Cl (0.234 g, 0.95 mmol) and N(H)diene (1.03 ml, 9.5 mmol) yielded the ligand L1 as red oil. (0.20 g, 70% yield). FT-IR (ATR) (cm^{-1}): 932 (ν(S-N)), 1319, 1140 (ν(S=O)). ^{1}H NMR (CDCl₃, 400 MHz) δ (ppm): 7.38-7.40 (m, 1H, Ha), 7.34-7.37 (m, 1H, Hb), 6.93-6.95 (m, 1H, Hc), 4.23-4.31 (m, 4H, O-CH₂-CH₂-O), 2.99 (t, J = 5.5 Hz, 2H, CH₂), 2.81 (t, J = 5.6 Hz, 2H, CH₂), 2.72 (t, J = 5.5 Hz, 2H, CH₂), 2.62 (t, J = 5.6 Hz, 2H, CH₂). ^{1}H NMR (DMSO-d_6, 400 MHz) δ (ppm): 7.24-7.27 (m, 2H, Ha, Hb), 7.02-7.05 (m, 1H, Hc), 4.30-4.33 (m, 4H, O-CH₂-CH₂-O), 2.77 (m, 3H, CH₂), 2.66 (t, J = 5.82 Hz, 2H, CH₂), 2.52-2.55 (m, 3H, CH₂).

2.2.2.2. Synthesis of (N(SO₂)(4-Mebip)dienH ligand (L2)

As described in the general procedure, with 4-methylbiphenyl-4-SO₂Cl (0.56 g, 2.0 mmol) and N(H)diene (2.18 ml, 20.0 mmol) yielded the ligand L2 as a light yellow powder (0.658 g, 99% yield). FT-IR (ATR) (cm^{-1}): 913 (ν(S-N)), 1366, 1153 (ν(S=O)). ^{1}H NMR (DMSO-d_6, 400 MHz) δ (ppm): 7.83-7.89 (m, 4H, Ha/a', Hb/b'), 7.62-7.63 (m, 2H, Hc/c'), 7.31 (d, J = 7.28 Hz, 2H, Hd/d'), 2.82-2.85 (m, 2H, CH₂), 2.54-2.72 (m, 4H, 2CH₂), 2.45 (m, 2H, CH₂), 2.36 (s, 3H, CH₃).

2.2.3. Synthesis of [Pt(NSO₂R)dienH)Cl₂] complexes

A suspension of *cis*-Pt(DMSO)₂Cl₂ (0.15 g, 0.35 mmol) in methanol (20 ml) was treated with *N*(SO₂R)dienH ligand (0.35 mmol), and the reaction mixture was stirred for 24 h. The solid precipitate was collected on a filter, washed with water and diethylether and dried under vacuum.

2.2.3.1. Synthesis of [Pt(N(SO₂)(bzd)dienH)Cl₂]complex (C1)

A suspension of 0.200 mmol of *cis*-Pt(DMSO)₂Cl₂ in methanol was treated with (0.06 g, 0.20 mmol) *N*(SO₂)(bzd)dienH (L1) and the reaction mixture was stirred at room temperature for 24 h. The resultant yellow solid was collected on a filter, washed with water and diethyl ether, and dried under vacuum (0.02 g, 13% yield). FT-IR (ATR) (cm^{-1}): 932 (ν(S-N)), 1315, 1150 (ν(S=O)). ^{1}H NMR (DMSO-d_6, 400 MHz) δ (ppm): 7.64 (m, 1H, N3H), 7.26-7.29 (m, 2H, Ha, Hb), 7.07 (m, 1H, Hc), 6.84 (brs, 1H, N2H), 6.02 (brs, 2H, N1H), 4.31-4.32 (m, 4H, O-CH₂-CH₂-O), 3.39-3.67 (m, 4H, 2CH₂), 2.83-3.15 (m, 4H, 2CH₂).

2.2.3.2. Synthesis of [Pt(N(SO₂)(4-Mebip)dienH)Cl₂]complex (C2)

As described above, 0.15 mmol of *cis*-Pt(DMSO)₂Cl₂ was treated with (0.05 g, 0.15 mmol) *N*(SO₂)(4-Mebip)dienH (L2) and the reaction mixture was stirred at 50-55°C temperature for 18 h. The resultant light-yellow solid was collected on a filter, washed with water and diethyl ether, and dried under vacuum (0.02 g, 20% yield). FT-IR (ATR) (cm^{-1}): 924 (ν(S-N)), 1352, 1152 (ν(S=O)). ^{1}H NMR (DMSO-d_6, 400 MHz) δ (ppm): 7.84-7.89 (m, 4H, Ha/a', Hb/b'), 7.77 (t, J = 5.7 Hz, 1H, N3H), 7.65 (d, J = 8.1 Hz, 2H, Hc/c'), 7.32 (d, J = 8.0 Hz, 2H, Hd/d'), 6.90 (brs, 1H, N2H sol), 6.32 (brs, 1H, N2H), 6.05 (brs, 2H, N1H sol), 5.27-5.37 (brd, 2H, N1H), 2.97-3.23 (m, 4H, 2CH₂), 2.57-2.85 (m, 2H, CH₂), 2.36 (s, 3H, CH₃), 2.21-2.33 (m, 2H, CH₂).

2.2.3.3. Synthesis of [Pt(N(SO₂)(1-nap)dienH)Cl₂]complex (C3)

The ligand *N(SO₂)(1-nap)dienH (L3)* was synthesized by following a reported procedure (Darshani et al., 2020a). A suspension of 0.20 mmol of *cis*- Pt(DMSO)$_2$Cl$_2$ in methanol was treated with (0.06 g, 0.20 mmol) *N*(SO$_2$)(1-nap)dienH and the reaction mixture was stirred at 50-55°C for 16 h. The resultant dark yellow solid was collected on a filter, washed with water and diethyl ether, and dried under vacuum (0.014 g, 12% yield). FT-IR (ATR) (cm^{-1}): 935 (ν(S-N)), 1316, 1159 (ν(S=O)). ^{1}H NMR (DMSO-d_6, 400 MHz) δ (ppm): 8.62 (d, J = 8.0 Hz, 1H, Hg), 8.26 (d, J = 8.2 Hz, 1H, Ha), 8.15-8.18 (m, 2H, Hc), 8.13 (m, 1H, N3H overlapped), 8.10-8.13 (m, 1H, Hd), 7.64-7.76 (m, 3H, Hb, He, Hf), 6.88 (brs, 1H, N2H), 6.03 (brs, 2H, N1H), 3.37-3.43 (m, 4H, 2CH$_2$), 3.16-3.2 (m, 2H, CH$_2$), 2.66-2.91 (m, 2H, CH$_2$).

2.2.3.4. Synthesis of [Pt(N(SO₂)(2-nap)dienH)Cl₂]complex (C4)

The ligand *N(SO₂)(2-nap)dienH (L4)* was synthesized by following a reported procedure (Darshani et al., 2020a). A suspension of 0.20 mmol of *cis*-Pt(DMSO)$_2$Cl$_2$ in methanol was treated with (0.06 g, 0.20 mmol) *N*(SO$_2$)(2-nap)dienH and the reaction mixture was stirred at room temperature for 24 h. The resultant light brown solid was collected on a filter, washed with water and diethyl ether, and dried under vacuum (0.05 g, 44% yield). FT-IR (ATR) (cm^{-1}): 980 (ν(S-N)), 1313, 1153 (ν(S=O)). ^{1}H NMR (DMSO-d_6, 400 MHz) δ (ppm): 8.53 (s, 1H), 8.15-8.23 (m, 2H), 8.05-8.07 (m, 1H), 7.93 (m, 1H, N3H),7.82-7.85 (m, 1H), 7.67-7.74 (m, 2H), 6.91 (brs, 1H, N2H), 6.07 (brs, 2H, N1H), 3.32-3.43 (m, 4H, 2CH$_2$), 2.73-3.19 (m, 4H, 2CH$_2$).

2.3. Biological studies

2.3.1. Prediction of drug-likeness

The drug-likeness of the synthesized ligands was determined by evaluating the properties specified in Lipinski's "Rule of 5". Molinspiration (www.molinspiration.com) (Karthick et al., 2013) server was used to determine parameters including molecular weight, hydrogen bond acceptors, hydrogen bond donors, water partition coefficient, molecule polar surface area, and the number of rotatable bonds.

2.3.2. Identification of potential targets

The potential targets for the four ligands were predicted via SwissTargetPrediction (Daina et al., 2019). It is possible to identify potential proteins which can interact with the desired molecule. These forecasts provide a fundamental understanding of the bio study and which biomolecules we should work with.

2.3.3. Cell culture and assessment of cytotoxic effects

Human non-small lung cancer cell line (NCI-H292) and human normal lung fibroblast cell line (MRC-5) were maintained in Dulbecco's Modified Eagle Medium (DMEM; Sigma Aldrich D5648) supplemented with 10% Fetal Bovine Serum (FBS) and 1% v/v penicillin-streptomycin. All the cells were maintained at 37° C in the incubator having humidified atmosphere with 5% CO$_2$(Darshani et al., 2020b, Maladeniya et al., 2022, Thushara et al., 2021).

Toxic effects exerted by the synthesized ligands and their platinum complexes on NCI-H292 and MRC-5 were assessed using Sulforhodamine B (SRB) assay. Briefly, seeded cells (5000 cells/200 μL) were treated with the synthetic compounds at 6.25, 12.5, 25, 50 and 100 μg/ml concentrations in 96-well culture plates. At 24, 48 and 72 h of post-treatment periods, cells were washed with phosphate buffer solution (PBS), then fixed with 10% trichloroacetic acid-DMEM for an hour at 4° C. Fixed cells were stained with 0.4% SRB. The SRB stain bound with the fixed cells was eluted with tris-base (10 mM, pH 7.5) at room temperature for 1h. The absorbance (Ab) was then measured at 540 nm using Synergy HTBioTek microplate reader. Percentage of cell viability (% CV) was calculated by using the equation: % CV= [(Ab$_{test}$ − Ab$_{blank}$)/(Ab$_{control}$ − Ab$_{blank}$)]x100.IC$_{50}$ values were calculated andnon-linear regression

analysis for log inhibitor vs. inhibition response (Dose-response, least square-ordinary fit) with variable slopes were performed using the software GraphPad Prism 8.0 (GraphPad software Corporation, Inc, San Diego, California, USA).The goodness of fit (R square) was maintained at $\geq$ 0.9. The software uses the experiment values of cell viability vs. concentration to determine Hillslope values of the curve. According to the Hillslope values, Prism 8.0 software calculates best-fit IC_{50} values.

3. Results and Discussion
3.1. ^{1}H NMR characterization

The $N(SO_2R)$dienH ligands and the [Pt($N(SO_2R)$dienH)Cl$_2$] complexes reported here were characterized by ^{1}H NMR in DMSO-d_6 and occasionally in CDCl$_3$. Analyzing the splitting pattern and integration resulted in the assignment of NMR signals. In order to observe the solvolysis product of [Pt($N(SO_2)$(4-Mebip)dienH)Cl$_2$], ^{1}H NMR was performed seven days after the dissolution of C2. The aromatic portions of the L1 and L2 ligands were observed in the 6.95-7.90 ppm range of the spectra, while the aliphatic methylene protons of the dienH backbone were observed in the 2.45-2.99 ppm range. Coordination of a ligand typically results in a downfield ^{1}H NMR shift due to the metal inductive effect. Upon coordination to Pt of the free ligands L1 and L2 in DMSO-d_6, the downfield shift observed in C1 and C2 complexes, respectively. Similar results were detected in C3 and C4 complexes, comparing their chemical shifts with previously reported respective ligands $N(SO_2)$(1-nap)dienH and $N(SO_2)$(2-nap)dienH.(Darshani et al., 2020a) Immediately upon dissolution of Pt complexes, NH signals were observed. Terminal N1H2 and central N2H signals appeared in the range of 5.00-6.00 ppm and 6.00-7.00 ppm as broad singlets, respectively, while N3H observed between 7.00-8.00 ppm as a broad triplet (Table 1, Figure 2 and Figure 3). The absence of NH signals in ^{1}H NMR spectra in DMSO-d_6 of synthesized L1 and L2 ligands are in agreement with Pt-N(sulfonamido) bond based study by Christoforou et al., which reports the similar kind of ligands; DHSN-dienH and their Pt(II) complexes (Christoforou et al., 2006).

Moreover, the coordination mode of $N(SO_2R)$dienH ligands with Pt has been established as bidentate mode unless alkaline conditions are used and lone pairs of terminal N1H$_2$ and central N2H participate in the coordination to Pt; whereas, N3H does not participate in chelation, which can be demonstrated by the appearance of broad triplet (J_{H-H}= 5.3 Hz) (Christoforou et al., 2006) in the range of 7-8 ppm and confirm the formation of bidentate Pt complexes. Thus, our analysis of NH signals of L1, L2 ligands and C1-C4 complexes in comparison with that of Christoforu et al confirms the denticity as being bidentate.

In addition to the above ^{1}H NMR spectrum of [Pt($N(SO_2)$(4-Mebip)dienH)Cl$_2$] (C2) complex was observed with one major set and one minor set of NH signals immediately after dissolution in DMSO-d_6. The major NH set was assigned to non-solvated product, [Pt($N(SO_2)$(4-Mebip)dienH)Cl$_2$] (C2), while the minor set was assigned to the solvolysis product (C2-sol). Comparison of integration ratios of the major and minor sets, revealed that approximately 2/3 of the non-solvated product (C2) coexists with the solvated product (C2-sol) in the prepared ^{1}H NMR sample. The C2 was further analyzed upon seven days after the dissolution of C2 in DMSO-d_6 and only one set of NH signals was observed, merely due to the solvolysis product (C2-sol*; solvated C2 after seven days) (Figure 4). Further dissolution of C2 resulted in ~0.05 ppm downfield shift between the NH protons of C2-sol and C2-sol*. The solvated aromatic protons appeared after seven days of dissolution, and no significant ^{1}H NMR shift was found compared to aromatic protons of non-solvated species.
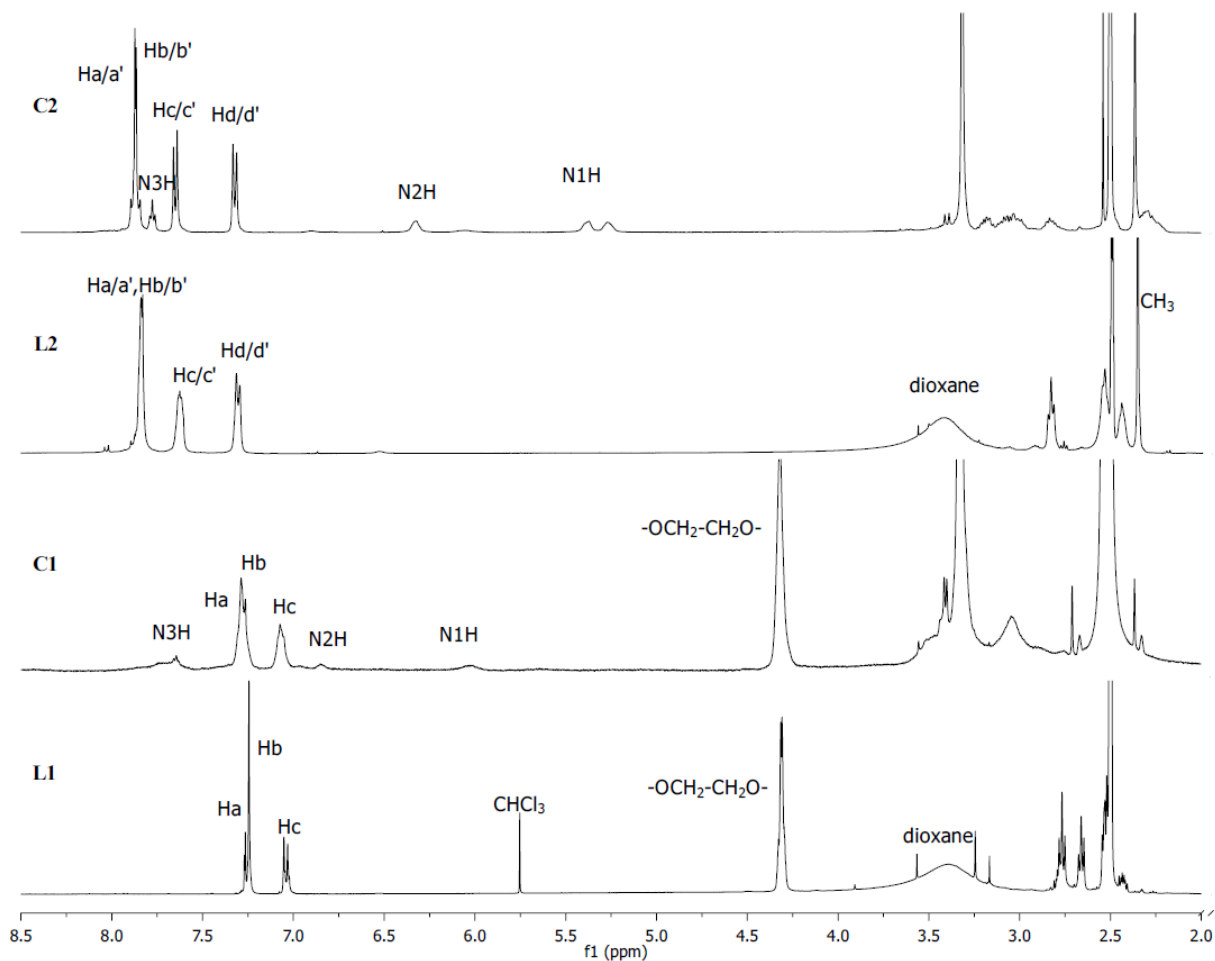
Figure 2. Selected regions of ^{1}H NMR spectra of N(SO$_2$)(bzd)dienH (L1), [Pt(N(SO$_2$)(bzd)dienH)Cl$_2$] (C1), N(SO$_2$)(4-Mebip)dienH (L2) and [Pt(N(SO$_2$)(4-Mebip)dienH)Cl$_2$] (C2) in DMSO-d_6 at 25 °C.
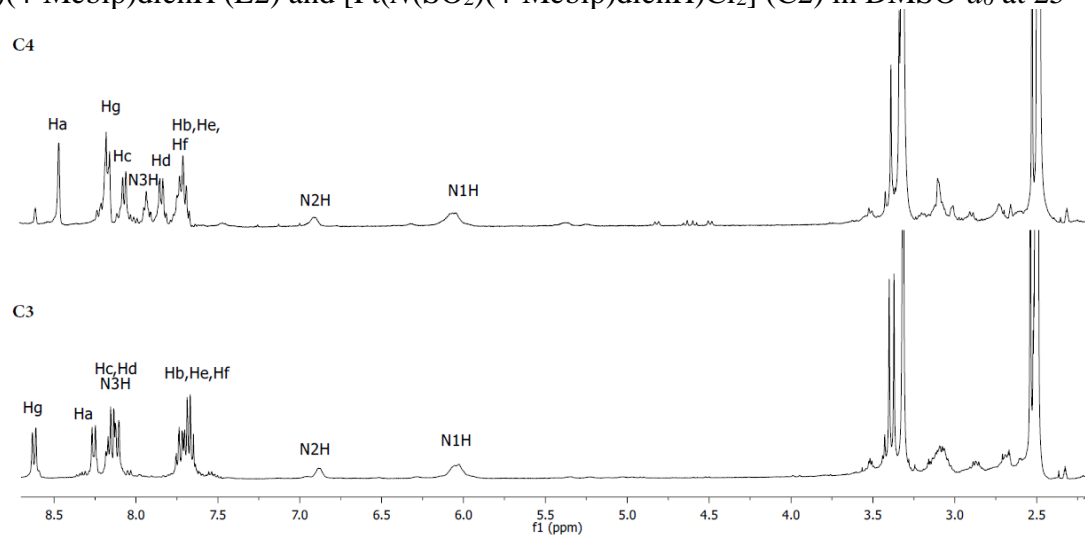
Figure 3. Selected regions of ^{1}H NMR spectra of [Pt(N(SO$_2$)(1-nap)dienH)Cl$_2$] (C3) and [Pt(N(SO$_2$)(2-nap)dienH)Cl$_2$] (C4) in DMSO-d_6 at 25 °C.

Table 1. ^{1}H NMR NH shifts (ppm) of Pt(II) complexes

		C1	C2	C2 -sol	C2 -sol*	C3	C4
H	N3	7.64	7.77	7.84	7.88	8.13 overlap	7.93
H	N2	6.84	6.32	6.90	6.95	6.88	6.91
H	N1	6.02	5.27 / -5.36	6.05	6.10	6.03	6.07

Figure 4. NH signals of [Pt(*N*(SO$_2$)(4-Mebip)dienH)Cl$_2$] (C2) complex in DMSO-*d$_6$*; seven days after dissolution (upper), Immediately upon dissolution (below).

Immediately after dissolution of C1, C3 and C4 in DMSO-*d$_6$*, only one major set of NH signals is observed. The NH1, NH2 and NH3 signal values of C1, C3 and C4 complexes (Table 1) are comparable to the ^{1}H NMR shift of solvolysis product of [Pt(DNSH-dienH)(Me$_2$SO-*d$_6$*)Cl]$^+$ previously reported. C1, C3 and C4 complexes, unlike C2, immediately produce their respective solvated forms in DMSO-*d$_6$*.

3.2. *FT-IR spectroscopy*
To establish the formation of the ligands and Pt(II) complexes, IR spectroscopic data obtained and the most significant IR data summarized in Table 2.

The ligands; L1 and L2 formation were verified by the presence of S-N stretching frequency and S=O stretching frequencies from the sulfone moiety. The newly formed S-N stretching frequency for *N*(SO$_2$)(bzd)dienH (L1) and *N*(SO$_2$)(4-Mebip)dienH (L2) are 932 cm^{-1} and 913 cm^{-1}(Darshani et al., 2020b), respectively and their Pt complexes also bear the same frequency. The asymmetric and symmetric S=O stretching vibrations of L1 and L2 arise at 1319 cm^{-1}, 1140 cm^{-1} and 1366 cm^{-1}, 1153 cm^{-1} respectively (Darshani et al., 2020b, Kaushalya et al., 2022). Confirming the structural features of pendent groups of ligands, C-H bending in 4-methyl group can be visualized at 807 cm^{-1} in L2, while C-O stretching peak of aliphatic ether of L1 is found at 1124 cm^{-1}(Silverstein and Bassler, 1962). The vibrational peaks between 3000-2850 cm^{-1} were assigned to the alkene C-H stretching vibrations of

ligands and complexes, whereas peaks around 1453-1458 cm^{-1} are due to aliphatic C-H bending vibrations (Silverstein and Bassler, 1962). Possibly due to an uncoordinated N-H bond, all bidentate Pt complexes (C1-C4) exhibit peaks in the range of 2359-2328 cm^{-1}, which were not detected in their respective ligands. Peaks in the range of 1650-1580 cm^{-1} are attributed to N-H bending (Silverstein and Bassler, 1962). However, the majority of ligand peaks appear in the spectra of new complexes, with minor shifts in peaks to higher or lower frequencies.

Table 2. The characteristic IR peaks of the ligands and the metal complexes in cm^{-1}

Ligand/ Complex	νS-N	$\nu_{as}(SO_2)$	$\nu_s(SO_2)$	N-H
L1	932	1319	1140	-
C1	932	1315	1150	2354, 2328
L2	913	1366	1153	-
C2	924	1352	1152	2360, 2339
L3	938	1316	1159	-
C3	935	1316	1159	2359, 2339
L4	953	1316	1152	-
C4	980	1313	1153	2359, 2328

3.3. UV-Visible and fluorometric analysis

Absorption spectra for the four ligands and four Pt(II) complexes were obtained in methanol at ambient temperature (Figure 5). Newly synthesized L1 and L2 ligands show high energy band between 200-300 nm due to intra-ligand transitions. L1 has three peaks; 212 nm attributed to n→π* transition while 245 nm and 285 nm arised due to intra-ligand π→π* transitions. In C1 complex, four peaks observed a slight bathochromic and hypsochromic shift at 207 nm, 218 nm, 243 nm and 292 nm upon NH coordination to Pt. There's no significant change in the absorption bands (205 nm and 270 nm) in C2 and L2, whereas a hypochromic shift observed at 270 nm in C2. The wavelengths of intense peaks are shifted towards lower wavelength ranges in both [Pt(N(SO$_2$)(1-nap)dienH)Cl$_2$] (C3) and [Pt(N(SO$_2$)(2-nap)dienH)Cl$_2$] (C4) complexes (Hypsochromic shift), a similar absorption behaviour reported in Re complexes (Darshani et al., 2020a). This may be due to alterations in the conjugated electron system when forming the new bonds between metal and ligand.

The emission spectra of ligands (L1-L4) and Pt complexes (C1-C4) were obtained in methanol at ambient temperature (Figure 6, Table 3). The concentrations of the test samples were approximately 0.5 mmol/dm^3 and slit width was maintained at 10 nm.
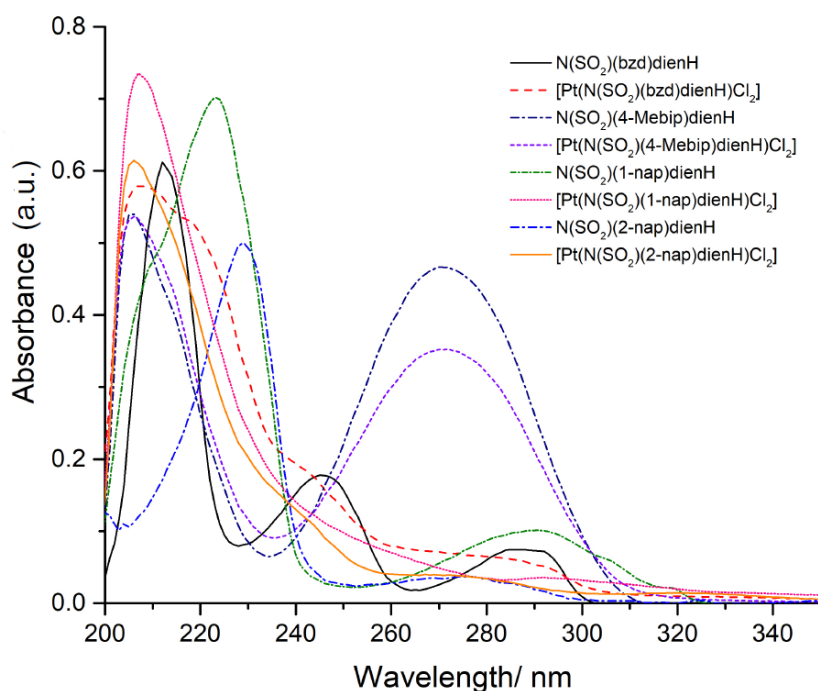
Figure 5. UV-Visible spectra of $N(SO_2)(bzd)dienH$ (L1), $[Pt(N(SO_2)(bzd)dienH)Cl_2]$ (C1), $N(SO_2)(4$-Mebip)dienH (L2), $[Pt(N(SO_2)(4$-Mebip)dienH)Cl_2]$ (C2), $N(SO_2)(1$-nap)dienH (L3), $[Pt(N(SO_2)(1$-nap)dienH)Cl_2]$ (C3), $N(SO_2)(2$-nap)dienH (L4) and $[Pt(N(SO_2)(2$-nap)dienH)Cl_2]$ (C4) in methanol at 298 K

Table 3. Excitation and emission data of the ligands and complexes in methanol at 298 K.

Test sample	Excitation wavelength/nm	Emission wavelength/nm
$N(SO_2)(bzd)dienH$	300	331
$[Pt(N(SO_2)(bzd)dienH)Cl_2]$	300	312
$N(SO_2)(4$-Mebip)dienH	310	364
$[Pt(N(SO_2)(4$-Mebip)dienH)Cl_2]$	310	362
$N(SO_2)(1$-nap)dienH	280	342
$[Pt(N(SO_2)(1$-nap)dienH)Cl_2]$	280	345
$N(SO_2)(2$-nap)dienH	280	333
$[Pt(N(SO_2)(2$-nap)dienH)Cl_2]$	280	311

Both the $N(SO_2)(bzd)dienH$ (L1) ligand and its Pt complex (C1) excited at 300 nm wavelength and emission were observed in the UV region with a blue shift (~19 nm) in the complex. The $N(SO_2)(4$-

Mebip)dienH (L2) displays higher fluorescence intensity at a low concentration, whereas its Pt complex (C2) has quenched fluorescence properties. $N(SO_2)(1\text{-nap})$dienH and $N(SO_2)(2\text{-nap})$dienH ligands also show high fluorescence intensities. $[Pt(N(SO_2)(2\text{-nap})$dienH$)Cl_2]$ possess quenched fluorescence properties with a slight blue shift (~22 nm). The blue shift observed in the spectra of C1 and C4 could be described as a result of rigidifying of the ligand and participation of lone pair of amino nitrogens with the metal cation. We may assign L2 as the best fluorophore based on the fluorescence properties of the ligands discussed here. All newly synthesized Pt complexes show low fluorescence intensity in contrast to that of the ligands indicating quenching of fluorescence upon metal complexation. This behaviour is similar to those observed for Re complexes derived by L3 and L4(Darshani et al., 2020b).
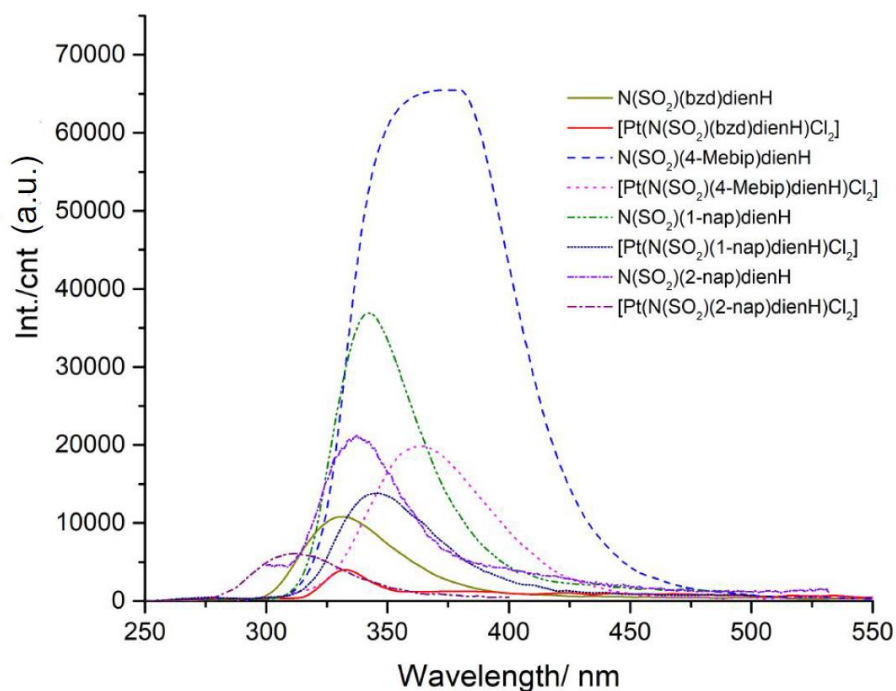
Figure 6. Fluorescence spectra of $N(SO_2)$(bzd)dienH (L1) (0.5 mM), $[Pt(N(SO_2)$(bzd)dienH$)Cl_2]$ (C1) (0.5 mM), $N(SO_2)$(4-Mebip)dienH (L2) (0.5 mM), $[Pt(N(SO_2)$(4-Mebip)dienH$)Cl_2]$ (C2) (0.5 mM), $N(SO_2)$(1-nap)dienH (L3) (0.5 mM), $[Pt(N(SO_2)$(1-nap)dienH$)Cl_2]$ (C3) (0.5 mM), $N(SO_2)$(2-nap)dienH (L4) (0.5 mM), $[Pt(N(SO_2)$(2-nap)dienH$)Cl_2]$ (C4) (0.5 mM) in methanol at 298 K

3.4. Biological studies
3.4.1. Prediction of drug-likeness of ligands
When the ligands L1, L2, L3 and L4 were examined for drug-likeness, they conformed to the 'rule of 5'. For a compound to be an orally active drug, it should possess parameters MW $\leq$ 500, logP $\leq$ 5, hydrogen bond donors $\leq$ 5, hydrogen bond acceptors $\leq$ 10, polar surface area $\leq$ 150 Å^2, and rotatable bonds $\leq$ 10. The ligands L1, L2, L3, and L4 are all within the acceptable range, indicating that they could be used as drug leads in the future.
3.4.2. Target prediction
For L1, L3 and L4, several probable biological targets were identified using SwissTargetPrediction (http://www.swisstargetprediction.ch), (Daina et al., 2019) where the highest probability for a target is with acetylcholinesterase. Therefore, L1, L3, and L4 ligands can be

acetylcholinesterase inhibitors which are associated with the treatment of neurological disorders. L2 is the highest target for serine/tyrosine kinase enzyme. Furthermore, recent studies have shown AChE inhibitors can act as anticancer agents via cell apoptosis (Lazarevic-Pasti et al., 2017, Richbart et al., 2021) more specifically, towards lung cancers.

3.4.3.   In vitro cytotoxic effects

Of the compounds synthesized, only L2, C2 and C4 have exhibited notable cytotoxic effects against non-small cell lung cancer cells in dose and time-dependent manner (Table 4). Whereas complex C1 showed dose-dependent cytotoxicity at 48 and 72 h incubation periods and C3 showed cytotoxicity in cancer cells only after 72 h treatment period. Among these active compounds, N(SO$_2$)(4-Mebip)dienH (L2) ligand demonstrated the strongest cytotoxic effects in NCI-H292 cells followed by C2 with IC$_{50}$ values < 25 µg/mL (Figure 7). Although L2 depicted considerable toxic effects on normal lung cancer cells at 72 h treatment period, it did not impact any toxicity on the cells at 24 and 48 h treatment periods (Figure 8). By contrast, C2 and C4 complexes were not cytotoxic to normal lung cells tested. The same trends were observed for C1 and C3 treatments. The morphological observations of the treated cancer and normal lung cells were further validating the cytotoxic potential of the synthesized compounds (Figures 7 and 8).

Table 4. IC$_{50}$ concentrations of ligands and their Pt complexes on NCI-H292 and MRC-5 cells after 24, 48 and 72 h of treatment periods.

Ligands (L)/Pt complexes (C)	IC$_{50}$ values (µg/mL)					
	NCI-H292			MRC-5		
	24 h	48 h	72 h	24 h	48 h	72 h
L1	148.50	141.80	135.20	845.30	775.80	620.10
C1	225.60	**45.36**	**40.14**	686.70	580.10	504.30
L2	**7.17**	**0.51**	**0.30**	221.90	176.90	**31.73**
C2	**22.56**	**21.25**	**19.08**	2494.00	1271.00	482.10
L3	209.38	1074.03	3325.04	**50.04**	134.13	161.53
C3	208.90	107.20	**16.27**	6720.00	2723.00	1223.00
L4	230.25	>1000	>1000	**48.81**	199.19	151.07
C4	**41.51**	**36.33**	**30.95**	388.40	153.40	151.30

a. Untreated NCI-H292 cells
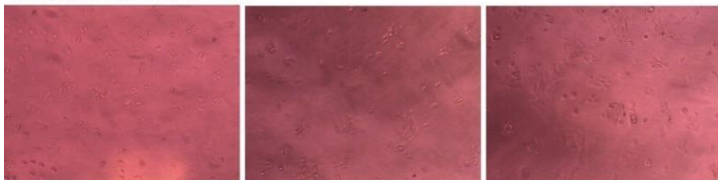
A – 24 h   B – 48 h   C – 72 h

b. L1   (A) 6.25 µg/mL   (B) 12.5 µg/mL   (C) 25 µg/mL   (D) 50 µg/mL   (E) 100 µg/mL
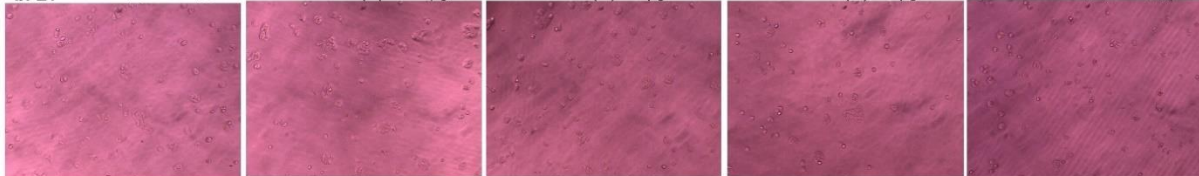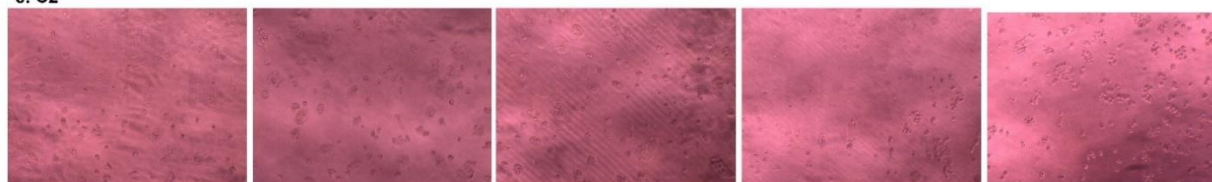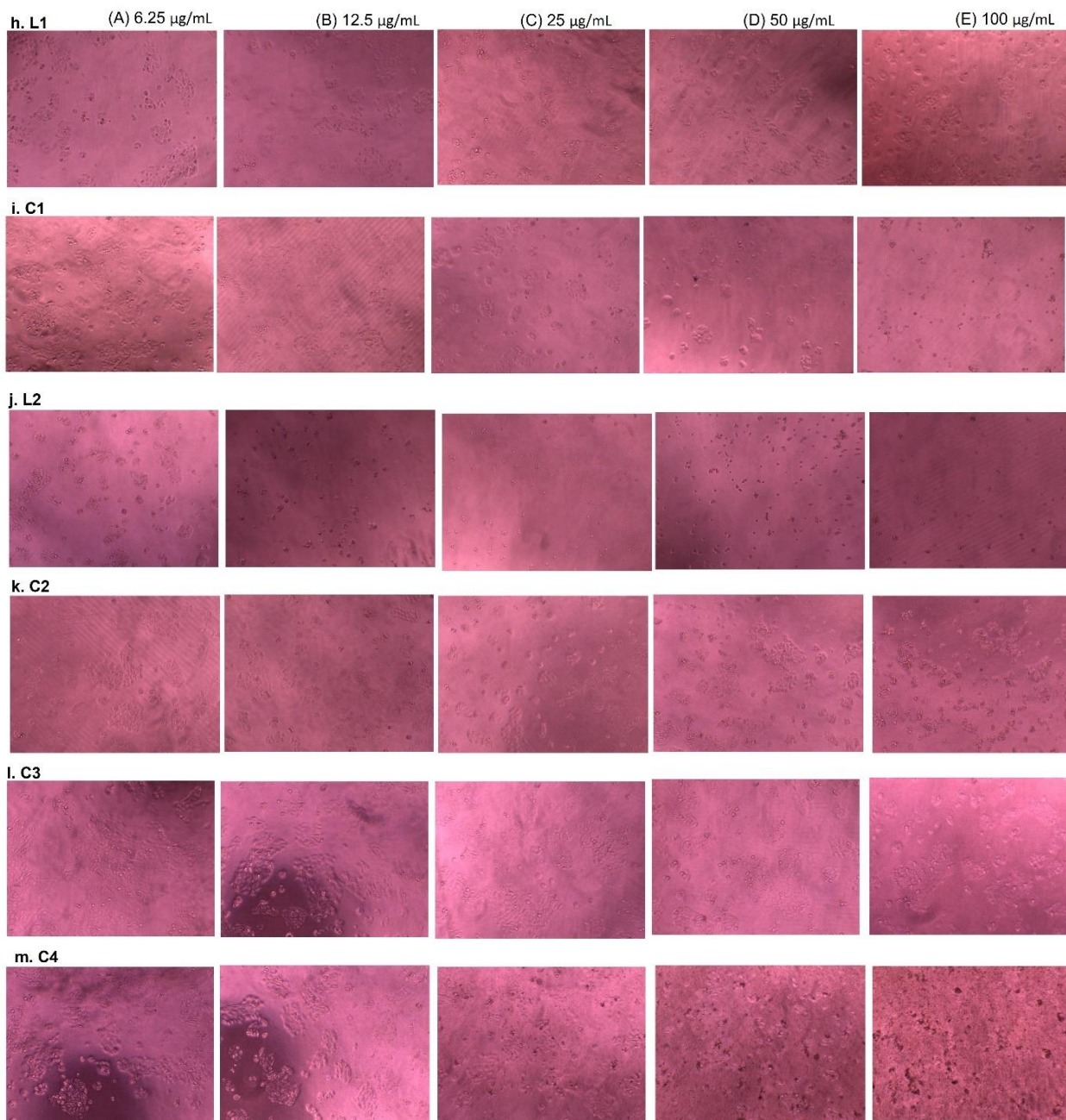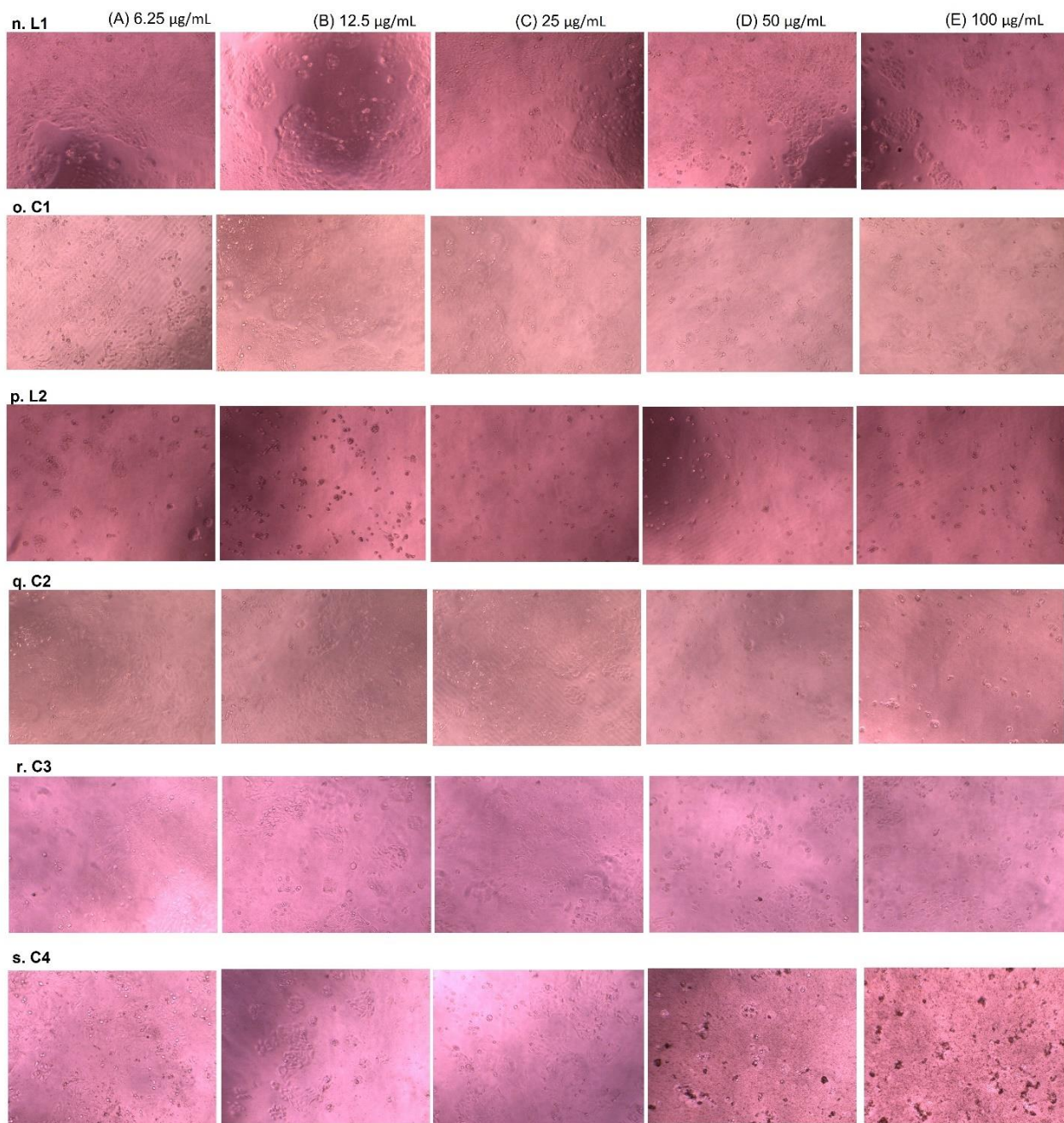
c. C1
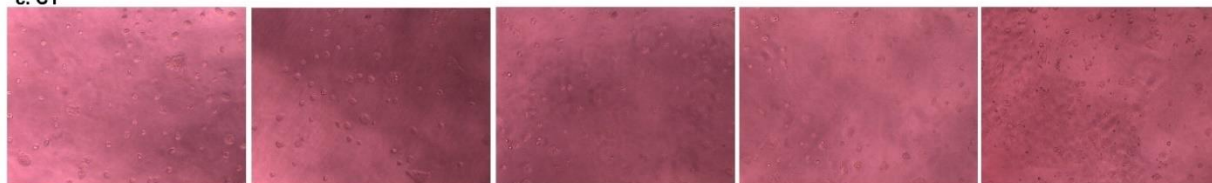
d. L2
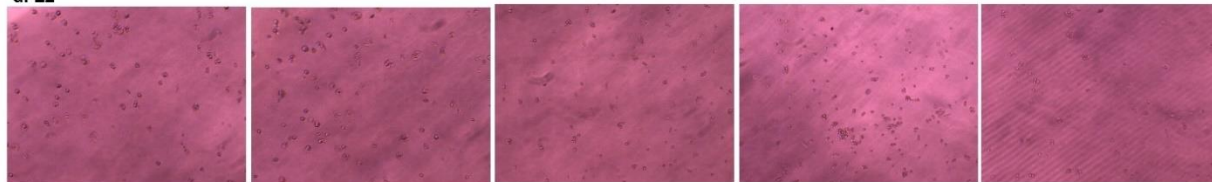
e. C2

f. C3

g. C4

Figure 7. Observations on morphological changes of the non-small cell lung cancer cells (NCI-H292) treated with ligands and their platinum complexes for 24 h (b-g), 48 h (h-m) and 72 h (n-s) and the respective untreated cells (a) (magnification at X 40).
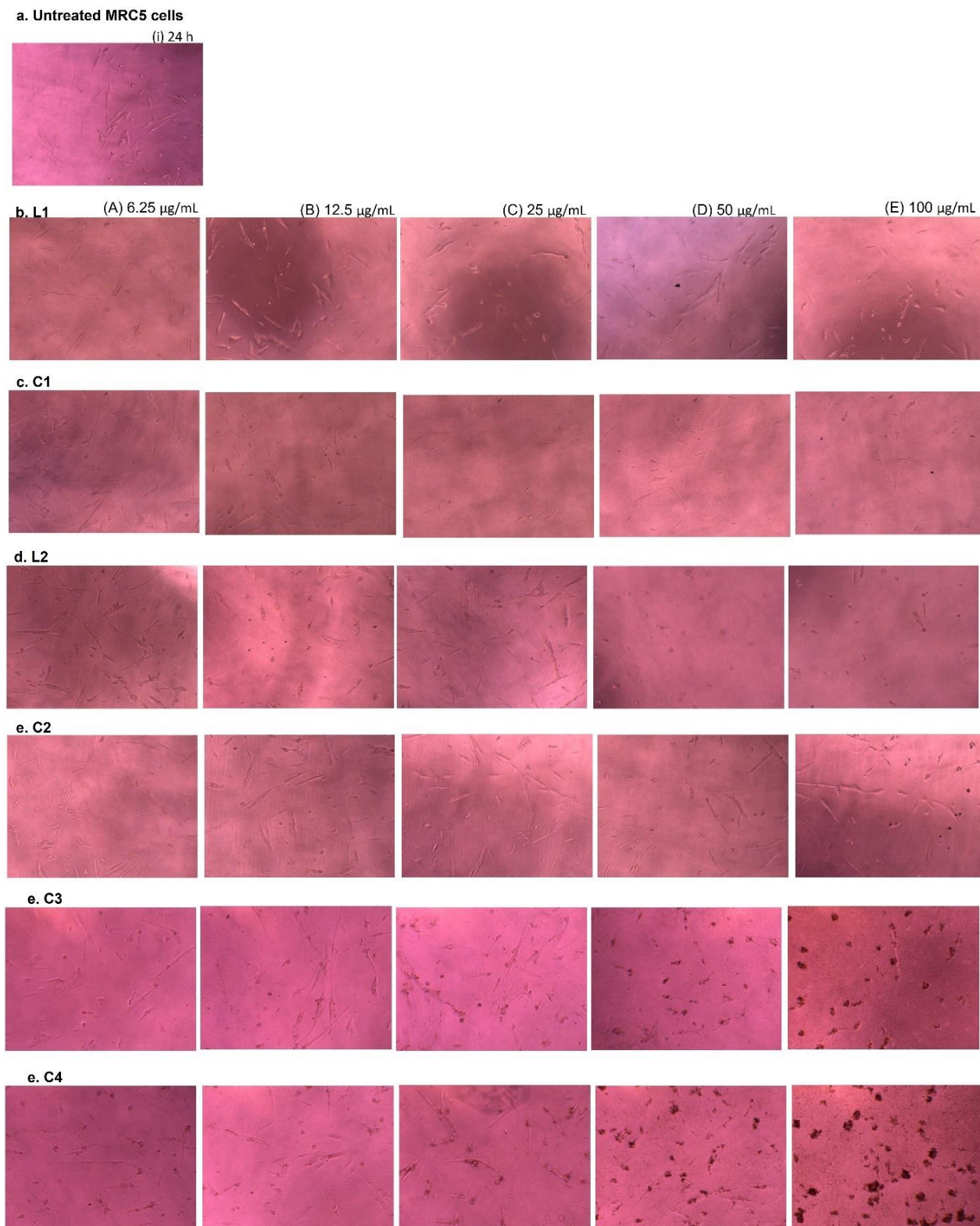
Figure 8. Morphological observations of the human healthy lung cells (MRC-5) treated with ligands and their Pt complexes (b-e) and the untreated cells (a) at 24 h post-incubation period (magnification at X 40).
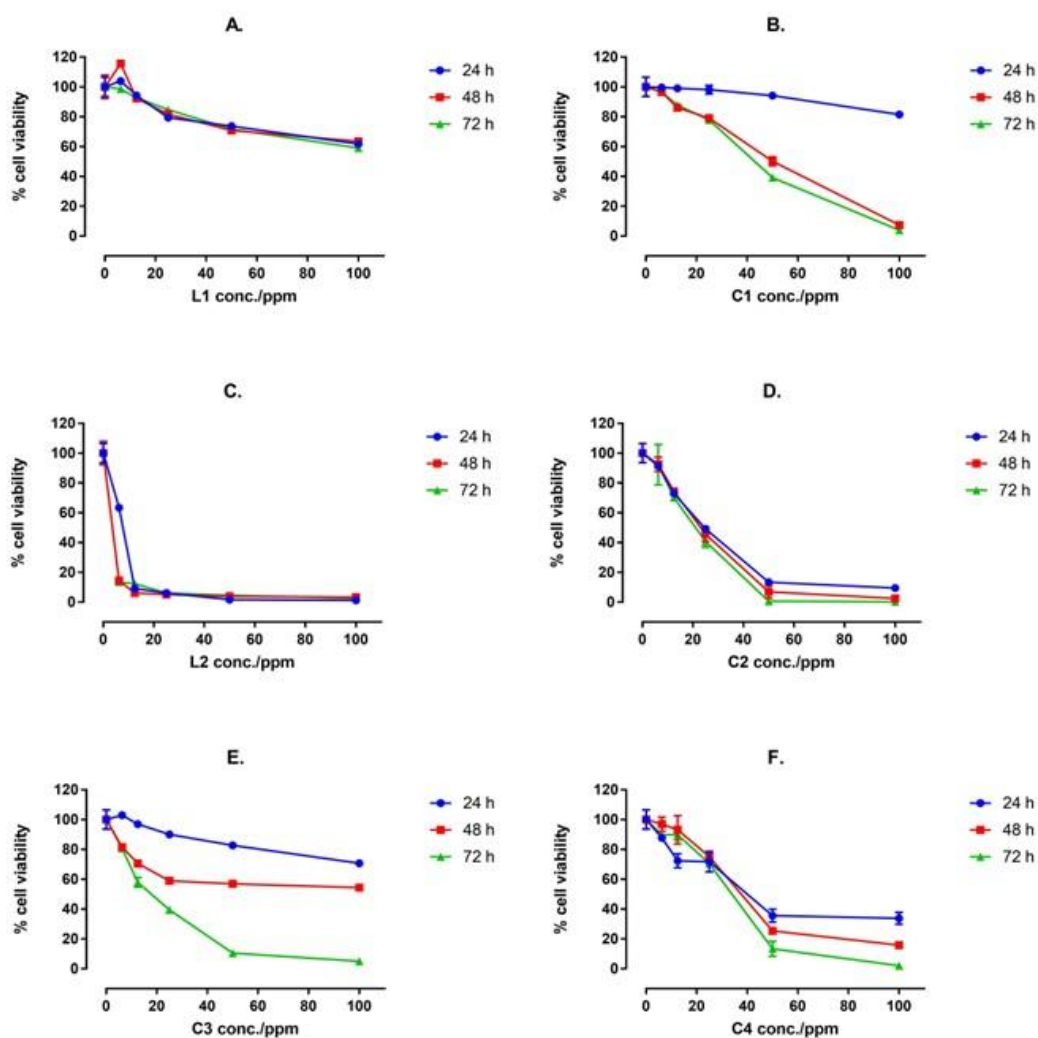
Figure 9. Cytotoxic effects of ligands their Pt metal complexes in NCI-H292 cells at 24 h, 48 h and 72 h post-treatment. The inhibition trend of (A.) L1, (B.) C1, (C.) L2, (D.) C2, (E.) C3, and (F.) C4 were plotted against their concentrations (6.25, 12.5, 25, 50 and 100 µg/mL).
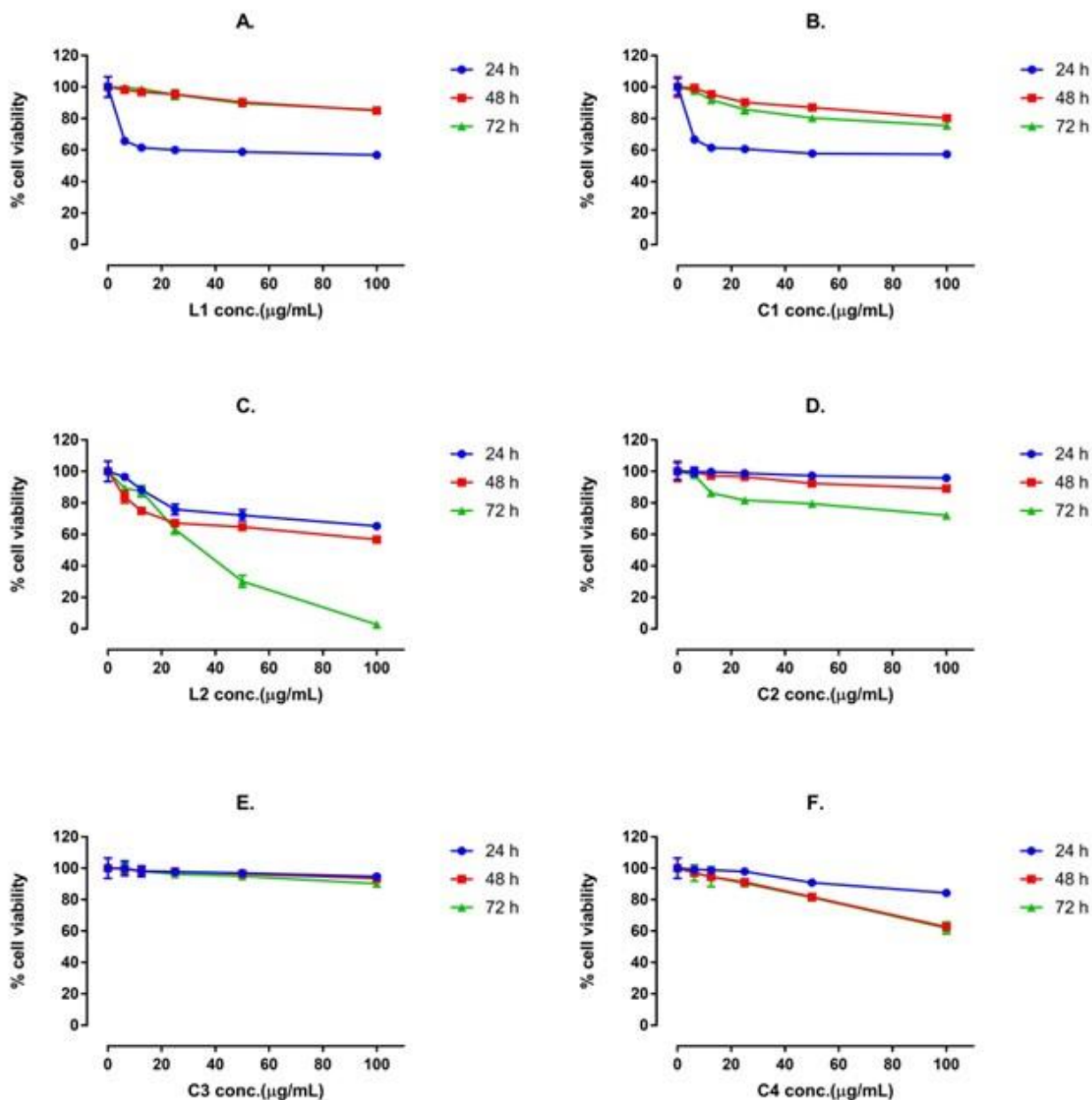
Figure 10. Cytotoxic effects of the ligands and their platinum complexes in MRC-5 cells after 24 h, 48 h and 72 h treatments. (A.) L1, (B.) C1, (C.) L2, (D.) C2, (E.) C3, and (F.) C4 treated at 6.25, 12.5, 25, 50 and 100 µg/mL concentrations.

4.   Conclusion

Two novel ligands (L1 and L2) and four novel Pt complexes (C1-C4) were synthesized and characterized by various spectroscopic techniques. The appearance of two broad peaks around 6.00-7.00

ppm confirms the ligand coordination with Pt and the appearance of a broad peak at 7.00-8.00 ppm indicates the bidentate mode of ligands vs tridentate mode. All four ligands showed high fluorescence intensities, but upon complexation, all Pt complexes show a quenching effect which may be due to the direct binding of ligand to metal. The target prediction suggested that L1, L3 and L4 have the highest probability for acetylcholinesterase enzyme and furthermore, AChE inhibitors possess the anticancer potential. The *in vitro* cytotoxic studies revealed that N(SO$_2$)(4-Mebip)dienH (L2) (<10 µg/mL), [Pt(N(SO$_2$)(4-Mebip)dienH)Cl$_2$] (C2) (<25 µg/mL)and [Pt(N(SO$_2$)(2-nap)dienH)Cl$_2$] (C4) (<50 µg/mL) are highly potent in suppressing the proliferation of non-small cell lung cancer cells with less or no cytotoxic impacts in normal lung cells, which warrants further investigating anti-proliferative effects and druggability of the platinum complexes. Our finding demonstrate that these compounds have the potential to be explored as drug leads for cancers.

Competing interests: The authors declare that they have no competing interests.

References:

Abhayawardhana, P. L., Marzilli, P. A., Fronczek, F. R. & Marzilli, L. G. J. I. C. 2014. Complexes possessing rare "tertiary" sulfonamide nitrogen-to-metal bonds of normal length: *fac*-[Re (CO)$_3$ (N (SO$_2$R) dien)] PF6 complexes with hydrophilic sulfonamide ligands. 53, 1144-1155.

Alemán, J., Del Solar, V., Alvarez-Valdés, A., Ríos-Luci, C., Padrón, J. M. & Navarro-Ranninger, C. J. M. 2011. Novel N-sulfonamide trans-platinum complexes: synthesis, reactivity and *in vitro* evaluation. 2, 789-793.

Chegwidden, W. R., Carter, N. D. & Edwards, Y. H. 2013. *The carbonic anhydrases: new horizons*, Birkhäuser.

Christoforou, A. M., Marzilli, P. A. & Marzilli, L. G. 2006. The Neglected Pt− N (sulfonamido) Bond in Pt Chemistry. New Fluorophore-Containing Pt (II) Complexes Useful for Assessing Pt (II) Interactions with Biomolecules. *Inorganic chemistry,* 45, 6771-6781.

Daina, A., Michielin, O. & Zoete, V. 2019. SwissTargetPrediction: updated data and new features for efficient prediction of protein targets of small molecules. *Nucleic acids research,* 47, W357-W364.

Darshani, T., Fronczek, F. R., Priyadarshani, V. V., Samarakoon, S. R., Perera, I. C. & Perera, T. 2020a. Synthesis and characterization of novel naphthalene-derivatized tridentate ligands and their net neutral rhenium tricarbonyl complexes and cytotoxic effects on non-small cell lung cancer cells of interest. *Polyhedron,* 114652.

Darshani, T., Fronczek, F. R., Priyadarshani, V. V., Samarakoon, S. R., Perera, I. C. & Perera, T. J. P. 2020b. Synthesis and characterization of novel naphthalene-derivatized tridentate ligands and their net neutral rhenium tricarbonyl complexes and cytotoxic effects on non-small cell lung cancer cells of interest. 187, 114652.

Farrell, N. 2003. Metal complexes as drugs and chemotherapeutic agents.

Fournel, M., Trachy-Bourget, M.-C., Yan, P. T., Kalita, A., Bonfils, C., Beaulieu, C., Frechette, S., Leit, S., Abou-Khalil, E. & Woo, S.-H. J. C. R. 2002. Sulfonamide anilides, a novel class of histone deacetylase inhibitors, are antiproliferative against human tumors. 62, 4325-4330.

Karthick, V., Ramanathan, K., Shanthi, V. & Rajasekaran, R. 2013. Identification of potential inhibitors of H5N1 influenza A virus neuraminidase by ligand-based virtual screening approach. *Cell biochemistry and biophysics,* 66**,** 657-669.

Kaushalya, C., Darshani, T., Samarakoon, S. R., Fronczek, F. R., Perera, I. C. & Perera, T. 2022. Synthesis, Characterization and Remarkable Anticancer Activity of Rhenium Complexes Containing Biphenyl Appended NNN Donor Sulfonamide Ligands.

Lazarevic-Pasti, T., Leskovac, A., Momic, T., Petrovic, S. & Vasic, V. J. C. M. C. 2017. Modulators of acetylcholinesterase activity: From Alzheimer's disease to anti-cancer drugs. 24**,** 3283-3309.

Maladeniya, C., Darshani, T., Samarakoon, S., Fronczek, F., Sameera, W., Perera, I., Perera, T. J. B. C. & Applications 2022. Biological Evaluation of Platinum (II) Sulfonamido Complexes: Synthesis, Characterization, Cytotoxicity, and Biological Imaging. 2022.

Mohan, R., Banerjee, M., Ray, A., Manna, T., Wilson, L., Owa, T., Bhattacharyya, B. & Panda, D. J. B. 2006. Antimitotic sulfonamides inhibit microtubule assembly dynamics and cancer cell proliferation. 45**,** 5440-5449.

Price, J. H., Williamson, A. N., Schramm, R. F. & Wayland, B. B. 1972. Palladium (II) and platinum (II) alkyl sulfoxide complexes. Examples of sulfur-bonded, mixed sulfur-and oxygen-bonded, and totally oxygen-bonded complexes. *Inorganic Chemistry,* 11**,** 1280-1284.

Richbart, S. D., Merritt, J. C., Nolan, N. A. & Dasgupta, P. J. A. I. C. R. 2021. Acetylcholinesterase and human cancers. 152**,** 1-66.

Rossi, A. & Di Maio, M. J. E. R. O. A. T. 2016. Platinum-based chemotherapy in advanced non-small-cell lung cancer: optimal number of treatment cycles. 16**,** 653-660.

Siegel, R. L., Miller, K. D., Wagle, N. S. & Jemal, A. J. C. A. C. J. F. C. 2023. Cancer statistics, 2023. 73**,** 17-48.

Silverstein, R. M. & Bassler, G. C. 1962. Spectrometric identification of organic compounds. *Journal of Chemical Education,* 39**,** 546.

Thushara, N., Darshani, T., Samarakoon, S. R., Perera, I. C., Fronczek, F. R., Sameera, W. & Perera, T. J. R. A. 2021. Synthesis, characterization and biological evaluation of dipicolylamine sulfonamide derivatized platinum complexes as potential anticancer agents. 11**,** 17658-17668.

Wang, D. & Lippard, S. J. 2005a. Cellular processing of platinum anticancer drugs. *Nature reviews Drug discovery,* 4**,** 307-320.

Wang, D. & Lippard, S. J. J. N. R. D. D. 2005b. Cellular processing of platinum anticancer drugs. 4**,** 307-320.

Wolff, M. E. J. A. J. O. T. 1996. Burger's medicinal chemistry and drug discovery. 3**,** 608.

Zhu, Z., Wang, Z., Zhang, C., Wang, Y., Zhang, H., Gan, Z., Guo, Z. & Wang, X. J. C. S. 2019. Mitochondrion-targeted platinum complexes suppressing lung cancer through multiple pathways involving energy metabolism. 10**,** 3089-3095.